 SDHM, vol.5, no.3, pp.251-273, 2009

Structures with Surface-Bonded PZT Piezoelectric Patches: a BEM Investigation into the Strain-transfer Mechanism for SHM applications

I. Benedetti[1], **A. Milazzo**[1] **and M.H. Aliabadi**[2]

Abstract: In this work a three-dimensional BEM model is used for the analysis of structures with cracks and surface bonded piezoelectric PZT patches used as strain sensors. The cracked structure is modelled by the dual boundary element method, which allows for accurate and reliable crack analysis, while the piezoelectric patch is analyzed by a finite element state-space approach, that embodies both the full electro-mechanical coupling and the suitable sensor's boundary conditions. The model is used to investigate the strain-transfer mechanism from an host elastic structure to the piezoelectric layer, taking into account the effect of the adhesive layer, as well as the mechanical interaction between the sensor and the measured field. Finally, a fast solver based on the use of the GMRES and the hierarchical matrices is employed to speed up the solution of some large scale BEM systems arising from structural health monitoring applications. The numerical tool has been used to investigate the sensitivity of sensors arrangements in three-dimensional damaged solids.

Keywords: Piezoelectric patches, Structural health monitoring, Fast dual boundary element method

1 Introduction

High levels of reliability and low life-cycle costs are primary concerns in the design and maintenance of civil, chemical, mechanical, aeronautic and aerospace structures. In recent years, the idea of using Structural Health Monitoring (SHM) strategies, instead of classical inspection methods, has emerged, showing advantages like reduced down-time, elimination of component tear-down and the potential prevention of failures during operations [Noor (2000), Staszewski, Boller, and Tomlison (2004)].

[1] Universitá di Palermo, Palermo, Italy.
[2] Imperial College London, London, UK.

The SHM approach is based on the real-time detection of structural damage by means of the so called damage signatures, consisting in adverse changes in some structural features, so to replace scheduled inspection cycles with a continuous monitoring system. In practice, the task of health monitoring is accomplished through a network of sensors and storage/computing units able to track the variables related to the structural response, such as strain, vibration, electrical conductivity and acoustic emission, which are affected by the presence of damage. From this point of view, SHM systems can be collocated in the broad range of the *smart structures* and their design and implementation rely upon the efficient integration of the sensor network with the structure and on the combination with appropriate electronics, modeling and control algorithms. Typical employable sensors for such tasks are strain gauges, accelerometers, fiber optics, piezoelectric films and piezoceramics [Van der Auweraer and Peeters (2003)].

Piezoelectric films and patches, in particular, are a widely used class of sensors because of their reliability and sensitivity. By exploiting the direct piezoelectric effect, i.e. the generation of an electric field as a consequence of a mechanical load, they are able to sense the structural deformation and provide its indirect measure through a variation of voltage or rate of variation of voltage [Chopra (2002)]. Piezoelectric sensors for SHM applications are usually employed in the form of small polyvinylidene fluoride (PVDF) films or thin lead zirconate titanate (PZT) monolithic wafers. While PVDF elements are mainly used for sensing applications, the stiffer PZT transducers can also be used for actuation purposes. They can be either bonded on the surface of the structure or embedded into the structure itself. Due to their small size, the gradient identification for damage detection applications is often based on the use of arrays of such micro-electro-mechanical systems (MEMS). Piezoelectric based sensing networks can be grouped into two classes: active and passive sampling systems. Active sampling techniques require externally supplied energy in the form of stress or electromagnetic waves and they lead to SHM based on the frequency response method or Lamb waves method. Passive sampling methods detect the structural response *perturbations* without the need of external energy injection. The typical passive sensing approach in SHM is strain measurement by piezolectric wafers [Rees, Chiu, and Jones (1992), Hautamaki, Zurn, Mantell, and Polla (1999), Chiu, Galea, L., and Rajic (2000)].

It is then apparent from above that the design of SHM systems is a strongly multidisciplinary task, involving a deep understanding of structural behavior, damage mechanics, sensors characteristics, signal processing and optimization theory. One of the key features enabling the design of such devices is the availability of reliable mathematical models for the analysis of sensors, actuators and the whole SHM systems.

A comprehensive bibliography about FEM and BEM modeling of sensors and ac-

tuators is given by Mackerle (1999). Some investigations have also been devoted to the analysis of piezoelectric layers bonded to isotropic [Zhang, Zhang, and Fan (2003), Ali, Mahapatra, and Gopalakrishnan (2004), Ali, Mahapatra, and Gopalakrishnan (2005)] and orthotropic [Huang and Sun (2006)] elastic substrates. Other works focus on the modeling of the whole SHM system, trying to take into account the various aspects comprising the damage identification strategy. Lin and Yuan (2001) proposed an analytical model for an isotropic plate with integrated piezoelectric actuators and sensors for Lamb waves based SHM systems. The detection of cracks in plates through piezo-generated Lamb waves is studied by Tua et al. (2001), who considered several system parameters and proposed a methodology for locating and quantifying the extent of cracks. Fukunaga et al. (2002) developed a two stage strategy for damage identification, using a limited number of piezoelectric devices. Liu et al. (2003) modeled the whole input-output behavior of composite plates with adhesively bonded piezo-sensors and actuators, using a dynamic one-dimensional piezoelectric model, thin plate orthotropic theory and multiple integral transforms. Liang and Hwu (2004) focused on the online identification of holes/cracks in a structure through static strain measures and artificial neural networks. Raghavan and Cesnik (2005) proposed a generic procedure to obtain the guided waves (GW) field excited by finite dimensions piezoelectric actuators bonded on an infinite isotropic plate. They also proposed a model for the response of the piezoelectric sensors in GW fields, considering them as infinitely compliant layers. Sumant and Maiti (2006) proposed a strain based technique to detect size and location of cracks in beam-like components through discrete PZT patches and validated a BEM model for such systems through experimental results. In this work the sensitivity of a strain passive sensing SHM system is investigated by a numerical model for the analysis of three-dimensional damaged solids with adhesively bonded piezoelectric patches [Benedetti, Aliabadi, and Milazzo (2009)]. The damaged structure is modeled and analyzed through a fast Dual Boundary Element Method (DBEM) based on the use of hierarchical matrices in conjunction with a GMRES iterative solver, previously developed by Benedetti, Aliabadi, and Daví (2008) for the analysis of large scale cracked structures. The DBEM allows to model with accuracy the presence of cracks and its performance in terms of memory storage and solution time is improved using the hierarchical solver. The attached sensors, as well as the adhesive layer, are modeled using a 3D state-space finite element approach [Quing, Qiu, and Liu (2006)], taking into account the full electro-mechanical coupling in the piezoelectric layer. The suitable boundary conditions are embodied in the sensor model which is eventually expressed in terms of interface variables, allowing straightforward coupling with the underlying host structure.

The paper is organized as follows. In section 2 the dual boundary element model

of the host structure is briefly reviewed and the main features of the hierarchical treatment for fast BEM solution are addressed. In section 3 the model for the structure with attached piezoelectric patches is introduced and the strategy for the fast solution of the complete system is presented. In section 4 the strain-transfer mechanism is deeply investigated with reference to a single sensor. The response of a cracked plate with bonded sensors is then computed to evaluate the sensitivity of different sensors arrangements to the crack size.

2 Host structure model

The numerical modeling of a whole SHM system relies upon the accurate and efficient evaluation of the response of the damaged host structure, to which the sensors are bonded. The DBEM provide a general and effective tool for analyzing both two-dimensional [Portela, Aliabadi, and Rooke (1992, 1993)] and three-dimensional [Mi and Aliabadi (1992, 1994)] crack problems in the framework of the BEMs [Aliabadi (1997b,a)].

2.1 Dual boundary element method

Referring to a cracked body, the DBEM is based on the use of two independent boundary integral equations, namely the displacement integral equations and the traction integral equations, [Portela, Aliabadi, and Rooke (1992)].
The displacement boundary integral equation is collocated on the external boundary where, assuming continuity of displacements at the boundary nodes, it takes the following form

$$c_{ij}(\boldsymbol{x}_0)u_j(\boldsymbol{x}_0)+\oint_\Gamma T_{ij}(\boldsymbol{x}_0,\boldsymbol{x})u_j(\boldsymbol{x})\,d\Gamma=\int_\Gamma U_{ij}(\boldsymbol{x}_0,\boldsymbol{x})t_j(\boldsymbol{x})\,d\Gamma \tag{1}$$

In Eq.(1), U_{ij} and T_{ij} represent the Kelvin displacement and traction fundamental solutions at the boundary point $\boldsymbol{x}$ when collocating at the point $\boldsymbol{x}_0$, c_{ij} are coefficients depending on the boundary geometry and computed through rigid body considerations and the symbol $\oint$ stands for Cauchy principal value integral related to the singularity of T_{ij}.
On the crack boundaries both the displacement and traction equations are used: the displacement equation is collocated over a crack surface, whereas the traction equation is collocated over the other one. When collocating the displacement boundary equation at the crack node $\boldsymbol{x}_0^-$, one obtains

$$\begin{aligned}c_{ij}(\boldsymbol{x}_0^-)u_j(\boldsymbol{x}_0^-)+c_{ij}(\boldsymbol{x}_0^+)u_j(\boldsymbol{x}_0^+)+\oint_\Gamma T_{ij}(\boldsymbol{x}_0^-,\boldsymbol{x})u_j(\boldsymbol{x})\,d\Gamma\\ =\int_\Gamma U_{ij}(\boldsymbol{x}_0^-,\boldsymbol{x})t_j(\boldsymbol{x})\,d\Gamma\end{aligned} \tag{2}$$

where $\boldsymbol{x}_0^-$ and $\boldsymbol{x}_0^+$ are the two coincident crack nodes belonging to the upper and lower crack faces, respectively. For smooth crack surfaces at the point $\boldsymbol{x}_0^-$, it results $c_{ij}(\boldsymbol{x}_0^-) = c_{ij}(\boldsymbol{x}_0^+) = (1/2)\delta_{ij}$.
The collocation of the traction integral equation at the crack lower surface point $\boldsymbol{x}_0^+$, where continuity of strains is assumed, provides

$$\begin{aligned} c_{ij}(\boldsymbol{x}_0^+)t_j(\boldsymbol{x}_0^+) - c_{ij}(\boldsymbol{x}_0^-)t_j(\boldsymbol{x}_0^-) + n_j(\boldsymbol{x}_0^+) \,\text{⨍}_\Gamma T_{ijk}(\boldsymbol{x}_0^+,\boldsymbol{x})u_k(\boldsymbol{x})\,d\Gamma \\ = n_j(\boldsymbol{x}_0^+)\int_\Gamma U_{ijk}(\boldsymbol{x}_0^+,\boldsymbol{x})t_k(\boldsymbol{x})\,d\Gamma \end{aligned} \tag{3}$$

where the kernels U_{ijk} and T_{ijk} contain derivatives of U_{ij} and T_{ij} respectively, n_j are the component of the outward normal at the point $\boldsymbol{x}_0^+$ and ⨍ stands for Hadamard principal value integral, originating from the singular nature of the kernel T_{ijk}.
Starting from the boundary integral equations (1), (2) and (3) the numerical model is obtained from a discretization of the external boundary and crack surfaces by suitable boundary elements fulfilling the continuity requirements of the formulation. In this work the discretization scheme adopted by Mi and Aliabadi (1992, 1994) is used. In particular, for the external boundary are used *continuous* eight-node quadratic elements whereas *discontinuous* eight-node quadratic elements are used for the modeling of *both* the crack surfaces.
After suitable numerical treatment the DBEM integral equations lead to the algebraic system

$$\boldsymbol{H}\boldsymbol{u} = \boldsymbol{G}\boldsymbol{t} \tag{4}$$

where $\boldsymbol{u}$ and $\boldsymbol{t}$ collect the nodal values of displacements and tractions, respectively. After enforcing the boundary conditions, the final linear algebraic system takes the form

$$\boldsymbol{A}\boldsymbol{x} = \boldsymbol{y} \tag{5}$$

where $\boldsymbol{x}$ is the vector of unknowns, the right hand side $\boldsymbol{y}$ stems from the application of the boundary conditions and the collocation matrix $\boldsymbol{A}$ contains the influence coefficients.

2.2 Fast solution of large DBEM system

When computations involve large systems, as in the case of SHM systems modeling, memory storage and time requirements, besides solution accuracy, become key elements for the choice of the numerical technique to be employed. The DBEM system of algebraic equations presents a coefficient matrix which is fully populated

and neither symmetric nor definite. This results in increased memory requirements as well as increased assembly and solution time with respect to other numerical methods for problems of numerical comparable size. In this context, the use of hierarchical matrices for the representation of BEM systems of equations, in conjunction with Krylov subspace iterative solution techniques, become a very appealing technique to speed up the computation maintaining the required accuracy and saving the storage memory needed for the collocation matrix treatment.

A fast solver for the analysis of three-dimensional DBEM elastic crack problems has been developed by the authors of the present work [Benedetti, Aliabadi, and Daví (2008), Benedetti, Milazzo, and Aliabadi (2009)]. The interested reader is referred to those works and the references therein for further details. here, only some basic concepts are recalled for the sake of completeness.

The fast BEM solver is based on the hierarchical representation of the collocation matrix [Bebendorf (2000)]. Such representation is built by representing the matrix itself as a collection of blocks, some of which admit a special approximated and compressed format. Such blocks, referred to as *low rank blocks*, can be approximated by computing only some of the entries of the original blocks through adaptive algorithms known as Adaptive Cross Approximation (ACA). A sufficient condition for the approximation to be valid is the asymptotic smoothness of the integral equations kernels [see e.g. Bebendorf and Grzhibovskis (2006)]. Low rank blocks represent the numerical interaction, through asymptotic smooth kernels, between sets of collocation points and clusters of integration elements which are sufficiently far apart from each other, see Fig. 1. The distance between clusters of elements enters a certain admissibility condition, based on some selected geometrical criterion, for the existence of a low rank approximant. The blocks that do not satisfy such condition are called *full rank blocks* and they need to be computed and stored entirely. The low rank representation of the collocation matrix allows to reduce the memory storage requirements as well as to speed up the operations involving the matrix, especially the matrix-vector multiplication which is the core operation in iterative solvers.

Once the hierarchical representation of the collocation matrix has been built, the solution of the system can be conveniently computed through iterative solvers, which take full advantage of the hierarchical representation by exploiting the efficiency of the low rank matrix-vector multiplication. The convergence of iterative solvers can be improved, or sometimes obtained from a non-convergent scheme, by using suitable preconditioners. In the present work a GMRES iterative solver [Saad and Schultz (1986)] with a hierarchical preconditioner is used for the solution of the system of equations. In the framework of the hierarchical representation a *coarse* preconditioner can be obtained by first generating a coarse approximation $\mathscr{A}(\varepsilon_p)$ of the original collocation matrix $\mathscr{A}(\varepsilon_c)$, where the relationship $\varepsilon_p > \varepsilon_c$ holds, ε

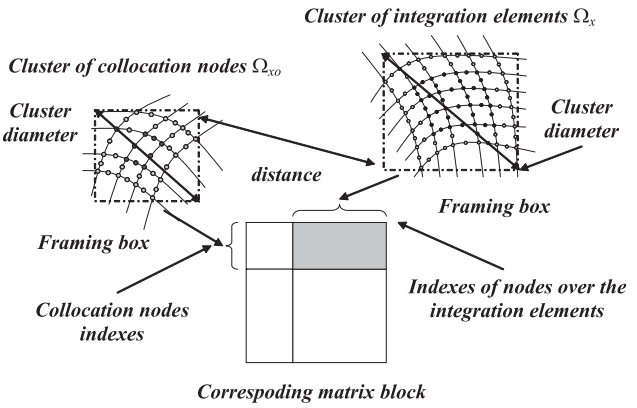

Figure 1: Correspondence between a matrix block and sets of collocation nodes and integration elements.

denoting the selected accuracy for the hierarchical representation. This coarse approximation, with reduced memory storage and required computation time, can then be decomposed through the hierarchical LU decomposition to give the preconditioner $\mathscr{L}\left[\mathscr{A}(\varepsilon_p)\right]^{-1}$ and build the final hierarchical system

$$\mathscr{L}\left[\mathscr{A}(\varepsilon_p)\right]^{-1}\mathscr{A}(\varepsilon_c)\boldsymbol{x} = \mathscr{L}\left[\mathscr{A}(\varepsilon_p)\right]^{-1}\boldsymbol{y} \tag{6}$$

The resolving system (6) has a lower condition number and can be solved by an iterative GMRES algorithm whose convergence rate results noticeably improved. Obviously, manipulations of the system require the use of a suitably defined arithmetic able to deal with matrices in hierarchical form [Hackbusch (1999); Hackbusch and Khoromskij (2000); S, Grasedyck, and Hackbusch (2003)].

3 Model for the structure with piezoelectric patches

In this section, the model for the static-strain piezoelectric sensor is briefly described, referring the reader to the work of Benedetti, Aliabadi, and Milazzo (2009) for the underlying formulation and required manipulations. The sensor model is based on a *state-space* formulation expressed in terms of the piezoelectric generalized variables [Lee and Jiang (1996), Sheng and Ye (2002)]. The state-space formulation gives the through-the-thickness patterns of suitably chosen structural variables in terms of the values of the same variables at a given reference plane. With reference to Fig. 2, for a piezoelectric wafer bonded to the host structure by

an adhesive layer, the state-space approach provides, after suitable discretization, the following relationship

$$\begin{bmatrix} \mathbf{u}_2 \\ \varphi_2 \\ \sigma_2 \\ \mathbf{D}_2 \end{bmatrix} = \begin{bmatrix} \mathbf{L}_{uu}(\Delta h_j) & \cdots & \mathbf{L}_{ud}(\Delta h_j) \\ \vdots & \ddots & \vdots \\ \mathbf{L}_{du}(\Delta h_j) & \cdots & \mathbf{L}_{dd}(\Delta h_j) \end{bmatrix} \begin{bmatrix} \mathbf{u}_0 \\ \varphi_1 \\ \sigma_0 \\ \mathbf{D}_1 \end{bmatrix} \tag{7}$$

where the subscripts refer to the corresponding level h_i and $\mathbf{u}_i$ collects the nodal displacements (at the height h_i), φ_i collects the nodal values of the electric potential, σ_i collects the nodal values of the out-of-plane stresses and $\mathbf{D}_i$ contains the out-of-plane electric displacement nodal values. The matrices $\mathbf{L}_{ij}(\Delta h_j)$ depend on $\Delta h_j = h_j - h_{j-1}$ with $j = 1,2$, and their expression can be found in [Benedetti, Aliabadi, and Milazzo (2009)].

When the piezoelectric wafer is used as a sensor, its surfaces are generally coated with a thin electrode and it can be then assumed that the surfaces h_1 and h_2 are equipotential. Moreover, it can be assumed, without loss of generality, that the inferior surface of the piezoelectric patch (h_1) is at zero electric potential and that the surface h_2 is stress-free. Consequently, applying open-circuit boundary conditions, from Eq.(7) one deduces the following relationships [Benedetti, Aliabadi, and Milazzo (2009)], which constitute the piezoelectric sensor model, written in the host structure reference system

$$\mathbf{t}(h_0) = \Psi\, \mathbf{u}(h_0); \tag{8}$$

$$\varphi(h_2) = \Phi\, \mathbf{u}(h_0) \tag{9}$$

Eq.(8) links the sensor nodal displacements $\mathbf{u}(h_0)$ and nodal tractions $\mathbf{t}(h_0)$ at the interface between the sensor and the host structure. This equation can be coupled

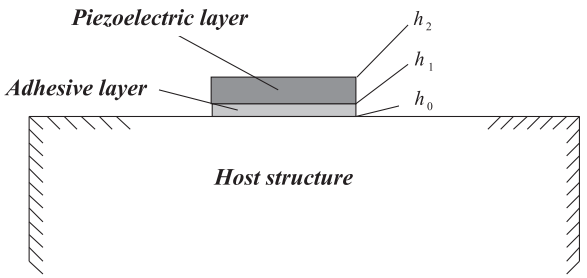

Figure 2: Piezoelectric sensor bonded on the host structure.

through standard interface conditions with the boundary element model of the host structure, allowing the computation of the unknowns $\mathbf{u}_0$. Once these values are known, Eq.(9) can be used for computing the sensor top surface electric potential $\varphi(h_2)$.
The presence of sensors bonded to the host structure is directly accounted for in the resolving system given in Eq.(5) according to the following observations. Let us partition the nodal displacements and tractions so that $\mathbf{u}_k^h$ and $\mathbf{t}_k^h$ denote displacements and tractions at the nodes of the host structures belonging to the interface with the *k-th* piezoelectric sensor, whereas $\mathbf{u}$ and $\mathbf{t}$ refer to the remaining surface. Invoking the interface continuity conditions between the host structure and the sensors and taking Eq.(8) into account, the algebraic system can be written as

$$\mathbf{H}\,\mathbf{u} + \sum_k (\mathbf{H}_k + \mathbf{G}_k \Psi_k)\mathbf{u}_k^h = \mathbf{G}\,\mathbf{t} \tag{10}$$

where the sum is extended over all the bonded sensors. After completing the application of the boundary conditions, the previous system assumes the form

$$\boldsymbol{A}\,\boldsymbol{x} + \sum_k \mathbf{G}_k \Psi_k\,\mathbf{u}_k^h = \boldsymbol{A}\,\boldsymbol{x} + \Phi_{pz}\boldsymbol{x}_{pz} = \boldsymbol{y} \tag{11}$$

where the vector $\boldsymbol{x}_{pz} \subset \boldsymbol{x}$ collects all the unknown displacements that multiply the columns belonging to the matrix Φ_{pz} introduced by the presence of the sensors. In Eq.(11) the collocation matrix related to the sole host structure appears and this shows that the presence of the piezoelectric patches affects such matrix only through the terms $\mathbf{G}_k\Psi_k$, which modify only some columns of the original collocation matrix itself. Once the displacements are obtained from the solution of Eq.(11), Eq.(9) allows the determination of the electric potential at the upper surface of the piezoelectric sensors.
The form of Eq.(11) suggests an efficient numerical scheme for its fast hierarchical solution. Since it can be reasonably assumed that the number of elements related to piezoelectric sensors is considerably less than the total number of boundary elements, the hierarchical counterpart of Eq.(11) is written as

$$\mathscr{A}\,\boldsymbol{x} + \Phi_{pz}\boldsymbol{x}_{pz} = \boldsymbol{y} \tag{12}$$

where $\mathscr{A}$ is the collocation matrix of the damaged structure without sensors expressed in hierarchical format, whereas Φ_{pz} is the matrix, expressed in full format, collecting the contributions related to the sensors. Since the presence of the sensors does not affect noticeably the structural behavior, the original preconditioner used in Eq.(6) is still efficient and can be used to improve the performance of the iterative solver. The validity of this consideration has been numerically demonstrated in

Table 1: Material constants for PZT4.

	C_{11}	C_{22}	C_{33}	C_{12}	C_{13}
GPa	139	139	115	77.80	74.30
	C_{23}	C_{44}	C_{55}	C_{66}	
	74.30	25.60	25.60	30.60	
	e_{31}	e_{32}	e_{33}	e_{24}	e_{15}
C/m^2	-5.20	-5.20	15.08	12.72	12.72
	k_{11}	k_{22}	k_{33}		
nFa/m	13.06	13.06	11.51		

[Benedetti, Aliabadi, and Milazzo (2009)]. The GMRES is then used for the rapid solution of the following system

$$\mathscr{L}\left[\mathscr{A}(\boldsymbol{\varepsilon}_p)\right]^{-1}(\mathscr{A}(\boldsymbol{\varepsilon}_c)\boldsymbol{x}+\Phi_{pz}\boldsymbol{x}_{pz})=\mathscr{L}\left[\mathscr{A}(\boldsymbol{\varepsilon}_p)\right]^{-1}\boldsymbol{y} \tag{13}$$

4 Numerical results and discussion

In this section, the numerical results obtained by using the present model are presented and commented. The response of an isolated sensor is first investigated and the effect of the adhesive layer is discussed. The response of the sensor attached to an host elastic substrate is then evaluated, highlighting the influence of the structure-sensor interaction on the measured output voltage. Some medium-scale structures with cracks and bonded piezoelectric sensors are finally analyzed, illustrating the use of the present numerical model in the framework of structural health monitoring applications.

4.1 Isolated sensor

First, the response of an isolated sensor to prescribed strains acting on its bottom surface is analyzed, see Fig. 3. The isolated sensor is generally comprised of a layer of piezoelectric material with thickness h_{pz} and an adhesive layer of thickness h_{adh}, that serves the purpose of bonding the piezoelectric patch to the host structure. The prescribed strains act on the inferior surface of this bi-layer system and, as it will be numerically shown, the presence of the adhesive layer has a critical influence on the sensor's sensitivity. The response of the sensor is given in terms of output voltage. Tab. 1 gives the values of the material constants for PZT4, while for the adhesive $G = 85\,MPa$ and $\nu = 0.33$.

The influence of the piezoelectric layer thickness is firstly investigated. The piezoelectric layer has size $10\,mm \times 10\,mm \times h_{pz}$ with h varying from $h_{min} = 0.1\,mm$ to

$h_{max} = 1\,mm$. No adhesive is considered in the first test and the strains $\gamma_x = \gamma_y = \gamma = 10^{-4}$ are applied directly to the basis of the piezoelectric layer. It is worth noting that this would be the case of a piezoelectric patch perfectly bonded on a substrate undergoing the prescribed strains γ_x and γ_y. In Fig. 4, the output voltage predicted by the present model is compared with that computed by using a simplified 2D model, in which the piezoelectric patch is modeled as an ideal capacitor, see for example the model used by Lin and Yuan (2001). The two responses match well with each other when the thickness of the considered layer is small with respect to the in-plane dimension. As the thickness increases, the three-dimensional effects related to the presence of shear strains at the sides of the piezoelectric layer become influent, thus affecting the output voltage in a way that is not predicted by the simplified 2D model.

The influence of the adhesive layer is then investigated. Fig. 5 reports the output voltage at varying values of the piezoelectric layer thickness h_{pz} for three different values of the adhesive layer thickness h_{adh}. The strains are prescribed at the basis of the adhesive layer. Various considerations can be made commenting on these results. First of all, it is evident that the output voltage is noticeably reduced as consequence of the presence of the adhesive layer, that affects the transmission of strains from the substrate to the piezoelectric layer. As can be observed from the comparison between Fig. 4 and Fig. 5, the presence of the adhesive layer reduces the output voltage of one or two order of magnitude. Moreover, while in Fig. 4 an increase of the piezoelectric layer thickness always implies an increase of the output voltage, the adhesive acts in such a way to make ineffective the increase of the thickness of the piezoelectric layer beyond a certain value. This is a consequence of the in-plane stiffness mismatch between the adhesive and the piezoelectric layer. As the thickness of the piezoelectric layer is increased, also its stiffness increases and the piezoelectric layer experiences a smaller deformation that is however am-

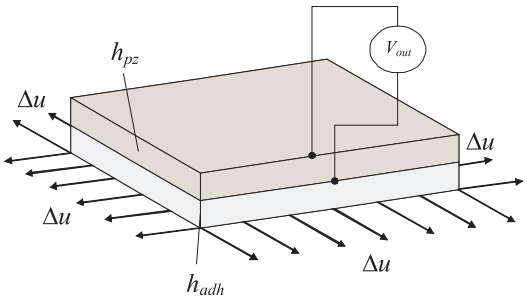

Figure 3: Isolated sensor subjected to prescribed strains.

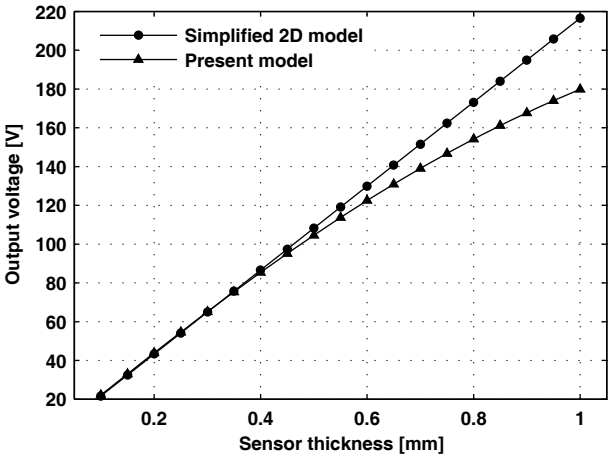

Figure 4: V_{out} versus h_{pz} in perfect-bonding conditions.

plified, in terms of output voltage, by the increased thickness itself. The increase of the thickness h_{pz} implies two counteracting effects: on one hand, it reduces the strain experienced by the piezoelectric layer, due to its superior stiffness; on the other hand, although the deformation is smaller, the higher thickness h_{pz} assures

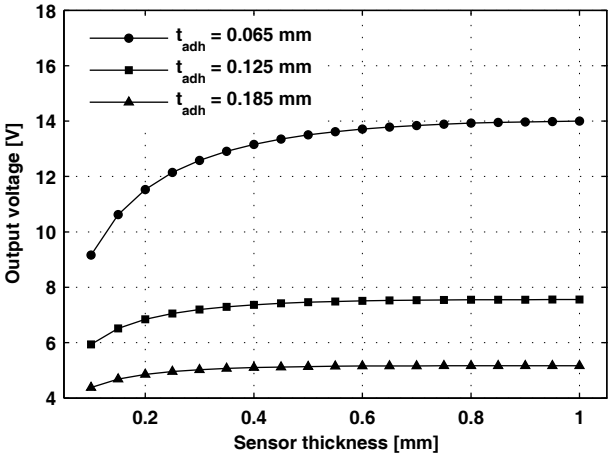

Figure 5: V_{out} versus h_{pz} for various values of the adhesive layer thickness t_{adh}.

an higher output voltage at a given strain level. These two counteracting effects cancel each other out beyond a certain value of h_{pz}, making then ineffective any additional increase of h_{pz} itself. This consideration can be particularly important if the piezoelectric sensors are to be used for lightweight applications.

The reduction of the sensor's sensitivity due to the presence of the adhesive layer is also show in Fig. 6, where the output voltage is expressed as a percentage of the voltage that the same piezoelectric layer would give in perfect-bonding conditions. As is evident, the quality of the bonding layer is a critical factor for the improvement of the sensor's sensitivity.

The influence of the sensor's in-plane size is investigated in Fig. 7, where the ratio between the output voltage predicted by the present model and that predicted by the simple 2D model is reported. The considered sensor has square in-plane shape $L \times L$, it is comprised of a piezoelectric layer of thickness $h_{pz} = 1\,mm$ and an adhesive layer of thickness h_{adh}, and its bottom surface is subjected to prescribed strains $\gamma_x = \gamma_y = 10^{-4}$. It is worth noting that the 2D model does not predict any dependence on the in-plane size of the patch, being the sensor modeled as an ideal capacitor perfectly bonded to the host structure. The present model, on the contrary, even in perfect-bonding conditions, predicts a certain dependence of the output voltage on the in-plane size when the ratio L/h_{pz} is low, due the the influence of the aforementioned 3D boundary shear effects. When the adhesive layer is present, the output voltage is reduced, but the response approaches the perfect-bonding re-

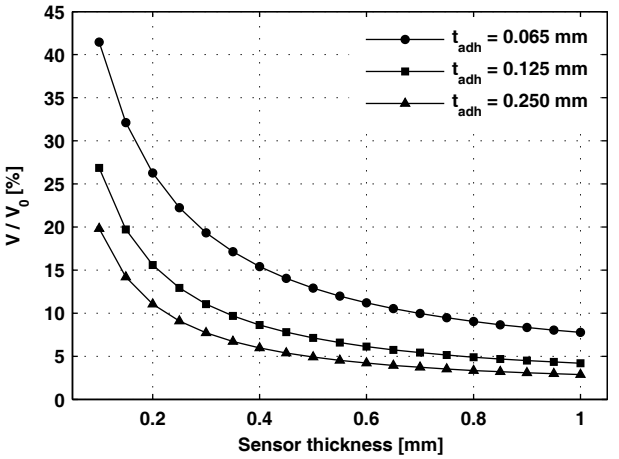

Figure 6: V_{out} versus h_{pz} as a percentage of the output voltage V_0 in perfect-bonding conditions.

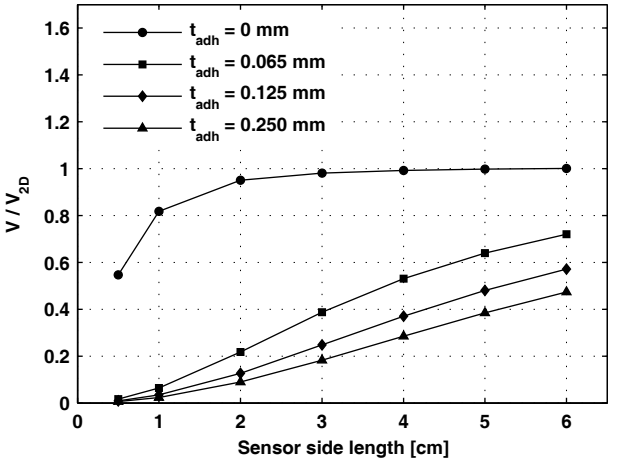

Figure 7: V_{out} versus L for various values of the adhesive layer thickness t_{adh}.

sponse as the ratio L/t_{adh} increases. This is due to the improvement of the strain transmission when the transmission surface increases in size.

4.2 Sensor bonded on an elastic substrate

After analyzing the isolated sensor, a sensor bonded on an elastic substrate is considered, Fig. 8. A piezoelectric patch of size $10\,mm \times 10\,mm \times 1\,mm$ is bonded on an aluminum plate of size $100\,mm \times 100\,mm \times t_{plate}$. The plate is subjected to uniform tractions $\sigma_x = \sigma_y = 10\,MPa$ acting along the four sides. The Young's modulus of the plate is $E = 72.5\,GPa$ while the Poisson's ratio is $\nu = 0.33$. The case of perfect bonding is first considered.

Fig. 9 reports: *a*) the output voltage of an *ideal* 2D sensor (the adjective ideal denotes a sensor that does not affect the strain field that it is revealing; in other words, there is no elastic interaction between the sensor and the host structure, the sensor is infinitely compliant and measures the strains that the structure would undergo if it were free to deform); *b*) the output voltage of an ideal sensor modeled with the proposed technique (note how the 3D shear effects reduce the voltage); *c*) the output voltage of a 3D sensor attached on a plate of thickness $t_{plate} = 20\,mm$; *d*) the output voltage of a 3D sensor attached on a plate of thickness $t_{plate} = 2\,mm$. It is evident as the elastic interaction between the sensor and the host structure affects the value of the output voltage. The deformation of the thinner plate in the area under the sensor, for example, is restrained by the presence of the sensor itself and this affects the output voltage. The deformation of the thicker plate, due to its supe-

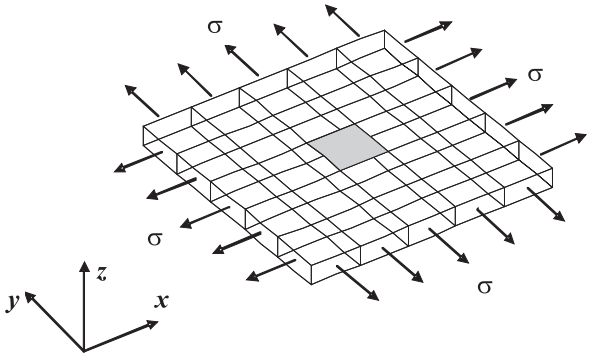

Figure 8: Sensor bonded on an elastic host structure.

rior transversal stiffness, is less affected by the presence of the sensor and the read voltage is higher. This aspect is particularly relevant when thin-plate structures are to be equipped with bonded piezoelectric sensor. The presence of the adhesive reduces the effect of the stiffness mismatch between the piezoelectric layer and the host structure on the output voltage, see Fig. 10, as the adhesive itself is a compliant layer.

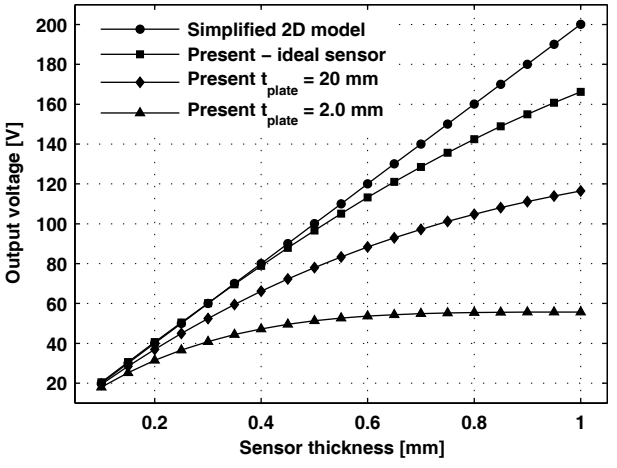

Figure 9: V_{out} versus h_{pz} for a sensor perfectly bonded on a host plate.

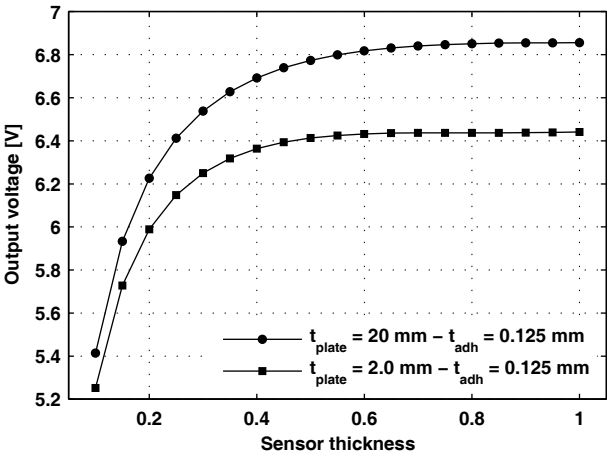

Figure 10: V_{out} versus h_{pz} for a sensor adhesively bonded on a host plate.

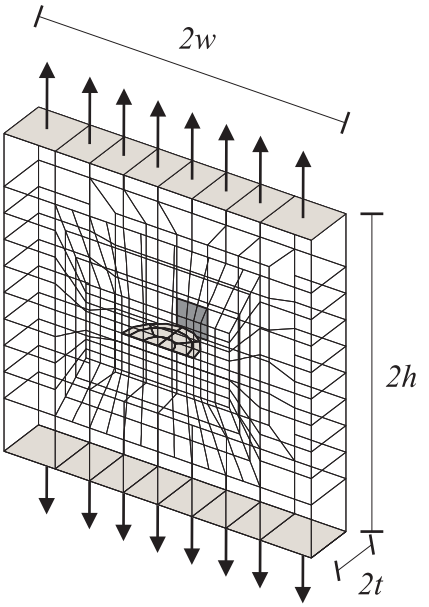

Figure 11: Semicircular surface-breaking crack in a plate under traction load.

4.3 Sensor bonded on a damaged substructure

In this section a medium-size structure with a crack and bonded piezoelectric patches used as sensors is analyzed. The case shown in Fig. 11 is considered. A semicir-

cular surface-breaking crack of radius a is contained in a plate of size $2w \times 2h \times 2t$ subjected to a crack-opening load and the face opposite to the cracked boundary surface is equipped with bonded sensors, see Fig. 12. Three different sets of sensors are considered, to investigate the sensitivity with respect to different crack/sensor relative positions. It is worth noting that the three different sets of sensors are considered independently from each other, to avoid the effects of interference on the output measured voltages. The plate dimensions are $w = h = 3\,cm$ and $t = 0.5\,cm$, the load is $\sigma = 10\,MPa$ and, to investigate the sensors response as the crack propagates through the thickness, the response of the sensors for the cases $a/2t = 0$, 0.1, 0.3, 0.5, 0.7, 0.9 are computed. The sensors have dimensions $L \times L \times h_{pz}$, with $L = 6\,mm$ and $h_{pz} = 0.5\,mm$. When present, the adhesive layer has thickness $h_{adh} = 0.125\,mm$. The used mesh has 1280 nodes and 381 elements and the computation has been carried out by using the fast hierarchical solver. For this medium-size mesh the solution has been computed in the 80% of time with respect to the standard procedures, and the coefficient matrix is stored using only 54% of the standard full rank storage memory. The performance in terms of solution time and storage memory is superior for larger scale systems, as demonstrated in Benedetti, Aliabadi, and Daví (2008); Benedetti, Milazzo, and Aliabadi (2009); Benedetti, Aliabadi, and Milazzo (2009), and this confirms the effectiveness of the fast BEM model for the analysis of SHM systems that tend to be inherently large-scale.

Fig. 13 reports the output voltage of the three sets of sensors at different crack sizes in the case of perfect bonding. As it can be noted, the sets A and B show a

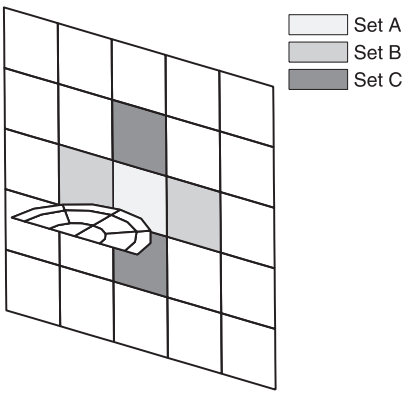

Figure 12: Relative position between the crack and the considered sensors' sets.

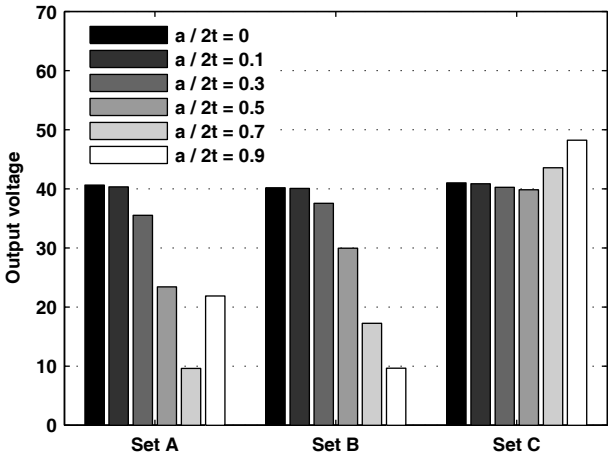

Figure 13: Output voltage for perfectly-bonded patches at different crack lengths.

superior sensitivity with respect to the crack size than the set C. It is worth noting that the voltage trend is affected by two counteracting strain effects: the first is related to the bending that the specimen experiences, due to the loss of symmetry

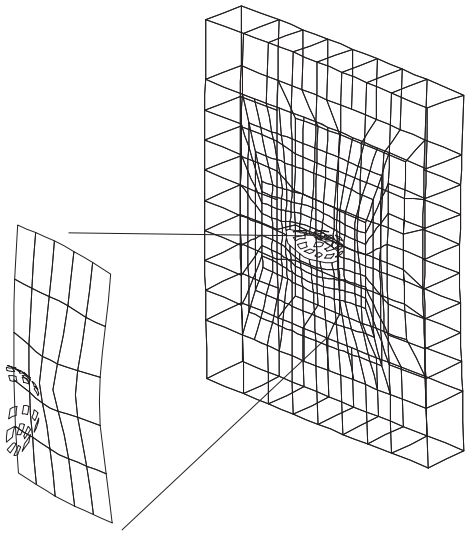

Figure 14: Deformed plate (amplified rendering).

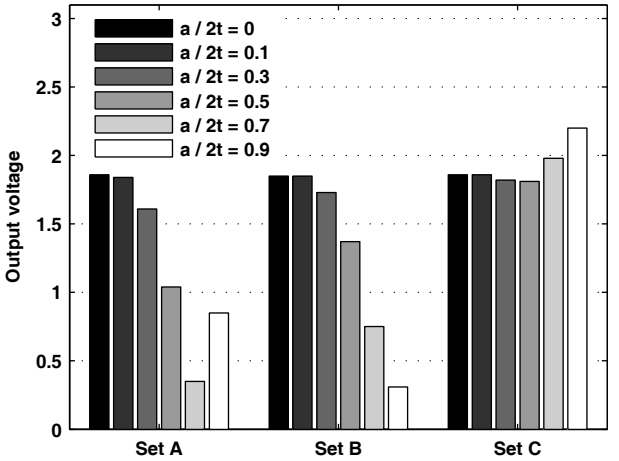

Figure 15: Output voltage for adhesively-bonded patches at different crack lengths.

under self balanced traction loads, responsible for a voltage drop with respect to the uncracked response; the second is related to the increase in stretching due to the reduced load bearing plate section, see Fig. 14. These effects are responsible for the behavior shown by the sensor A. The same trends are replicated in Fig. 15 where, however, a noticeable voltage level reduction results from the presence of the adhesive layer, thus confirming the critical importance of the adhesive layer quality.

5 Conclusions

In this work a BEM model was used to investigate the strain-transfer mechanism between a three-dimensional elastic host structure and surface bonded piezoelectric patches used as sensors. An in-depth investigation highlighted the influence on the output voltage of various factors: the shear related three-dimensional effects, the presence of the adhesive layer and the elastic interaction between the patch itself and the host elastic substrate. These effects, and especially the quality of the adhesive layer, have noticeable effects on the measured voltage and have to be taken into account in the design of this kind of SHM systems. Moreover, a plate with a surface-breaking crack and equipped with suitably arranged sets of sensors has been investigated. The obtained results showed that the sensors have different sensitivity to the crack presence and size, depending on their relative position with respect to it. In conclusion, however, it should be remarked that static-strain piezo-

electric patches are sensitive to the presence of cracks only when they are relatively close to them. Consequently, effective SHM systems based on these principles require, to be effective, the employment of quite fine networks of sensors over critical structural areas. Such networks have to be carefully designed and this requires the support of reliable and effective numerical models to assist any experimental campaign. The model used in this paper is a step towards in this direction.

References

Ali, R.; Mahapatra, D. R.; Gopalakrishnan, S. (2004): An analytical model of constrained piezoelectric thin film sensors. *Sensors and Actuators A*, vol. 116, pp. 424–437.

Ali, R.; Mahapatra, D. R.; Gopalakrishnan, S. (2005): Constrained piezoelectric thin film for sensing of subsurface cracks. *Sensors and Actuators A*.

Aliabadi, M. H. (1997): A new generation of boundary element methods in fracture mechanics. *International Journal of Fracture*, vol. 86, pp. 91–125.

Aliabadi, M. H. (1997): Boundary element formulations in fracture mechanics. *Applied Mechanics Reviews*, vol. 50, pp. 83–96.

Bebendorf, M. (2000): Approximation of boundary element matrices. *Numerische Mathematik*, vol. 86, pp. 565–589.

Bebendorf, M.; Grzhibovskis, R. (2006): Accelerating Galerkin BEM for linear elasticity using adaptive cross approximation. *Mathematical Methods in the Applied Sciences*, vol. 29, pp. 1721–1747.

Benedetti, I.; Aliabadi, M. H.; Daví, G. (2008): A fast 3D dual boundary element method based on hierarchical matrices. *International Journal of Solids and Structures*, vol. 45, pp. 2355–2376.

Benedetti, I.; Aliabadi, M. H.; Milazzo, A. (2009): A fast BEM for the analysis of damaged structures with bonded piezoelectric sensors. *Computer Methods in Applied Mechanics and Engineering*. doi:10.1016/j.cma.2009.09.007.

Benedetti, I.; Milazzo, A.; Aliabadi, M. H. (2009): A fast dual boundary element method for 3D anisotropic crack problems. *International Journal for Numerical Methods in Engineering*, vol. 80, pp. 1356–1378.

Chiu, W.; Galea, S.; L., K. L.; Rajic, N. (2000): Damage Detection in Bonded Repairs using Piezoceramics. *Smart Materials and Structures*, vol. 9, pp. 466–475.

Chopra, I. (2002): Review of state of art of smart structures and integrated systems. *AIAA Journal*, vol. 40, pp. 2145–2187.

C.Liang, Y.; Hwu, C. (2004): On-line identification of holes/cracks in composite structures. *Smart Materials and Structures*, vol. 13, pp. 643–660.

Fukunaga, H.; Hu, N.; Chang, F. K. (2002): Structural damage identification using piezoelectric sensors. *International Journal of Solids & Structures*.

Hackbusch, W. (1999): A sparse matrix arithmetic based on H-matrices. Part I: introduction to H-matrices. *Computing*, vol. 62, pp. 89–108.

Hackbusch, W.; Khoromskij, B. (2000): A sparse H-matrix arithmetic. Part II: application to multidimensional problems. *Computing*, vol. 64, pp. 21–47.

Hautamaki, C.; Zurn, S.; Mantell, S.; Polla, D. (1999): Experimental Evaluation of MEMS Strain Sensors Embedded in Composites. *Journal of Microelectromechanical Systems*, vol. 8, pp. 272–279.

Huang, G. L.; Sun, C. T. (2006): The dynamic behavior of a piezoelectric actuator bonded to an anisotropic elastic medium. *International Journal of Solids & Structures*.

Lee, J. S.; Jiang, L. Z. (1996): Exact electroelastic analysis of piezoelectric laminae via state space approach. *International Journal of Solids and Structures*, vol. 33, pp. 977–990.

Lin, X.; Yuan, F. G. (2001): Diagnostic Lamb waves in an integrated piezoelectric sensor/actuator plate: analytical and experimental studies. *Smart Materials and Structures*, vol. 10, pp. 907–913.

Liu, T.; Veidt, M.; Kitipornchai, S. (2003): Modelling the input-output behaviour of piezoelectric structural health monitoring systems for composite plates. *Smart Materials and Structures*, vol. 12, pp. 836–844.

Mackerle, J. (1999): Sensors and actuators: finite element and boundary element analyses and simulations. A bibliography (1997-1998). *Finite Elements in Analysis and Design*, vol. 33, pp. 209–220.

Mi, Y.; Aliabadi, M. H. (1992): Dual Boundary Element Method for three-dimensional fracture mechanics analysis. *Engineering Analysis with Boundary Elements*, vol. 10, pp. 161–171.

Mi, Y.; Aliabadi, M. H. (1994): Three-dimensional crack growth simulation using BEM. *Computers & Structures*, vol. 52, pp. 871–878.

Noor, A. K. (2000): *Structures Technology for Future Aerospace Systems*. American Institute of Aeronautics and Astronautics.

Portela, A.; Aliabadi, M. H.; Rooke, D. P. (1992): The Dual Boundary Element Method: effective implementation for crack problems. *International Journal for Numerical Methods in Engineering*, vol. 33, pp. 1269–1287.

Portela, A.; Aliabadi, M. H.; Rooke, D. P. (1993): Dual boundary element incremental analysis of crack propagation. *Computers & Structures*, vol. 46, pp. 237–247.

Quing, G.; Qiu, J.; Liu, Y. (2006): A semi-analytical solution for static and dynamic analysis of plates with piezoelectric patches. *International Journal of Solids & Structures*.

Raghavan, A.; Cesnik, C. E. S. (2005): Finite-dimensional piezoelectric transducer modeling for guided wave based structural health monitoring. *Smart Materials and Structures*, vol. 14, pp. 1448–1461.

Rees, D.; Chiu, W. K.; Jones, R. (1992): A Numerical Study of Crack Monitoring in Patched Structures using a Piezo Sensor. *Smart Materials and Structures*, vol. 1, pp. 202–205.

S, S. B.; Grasedyck, L.; Hackbusch, W. (2003): Introduction to hierarchical matrices with applications. *Engineering Analysis with Boundary Elements*, vol. 27, pp. 405–422.

Saad, Y.; Schultz, M. (1986): GMRES: a generalized minimal residual algorithm for solving nonsymmetric linear systems. *SIAM Journal on Scientific and Statistical Computing*, vol. 7, pp. 856–869.

Sheng, H. Y.; Ye, J. Q. (2002): A state space finite element for laminated composite plates. *Computer Methods in Applied Mechanics and Engineering*, vol. 191, pp. 4259–4276.

Staszewski, W. C.; Boller, C.; Tomlison, G. R. (2004): *Health Monitoring of Aerospace Structures - Smart sensor technologies and signal processing*. John Wiley & Sons Ltd.

Sumant, P. S.; Maiti, S. K. (2006): Crack detection in a beam using PZT sensors. *Smart Materials and Structures*, vol. 15, pp. 695–703.

Tua, P.; Quek, S. T.; Wang, Q. (2001): Detection of cracks in plates using piezo-actuated Lamb waves. *Smart Materials and Structures*, vol. 10, pp. 599–609.

Van der Auweraer, H.; Peeters, B. (2003): Sensors and systems for structural health monitoring. *Journal of Structural Control*, vol. 10, pp. 117–125.

Zhang, J.; Zhang, B.; Fan, J. (2003): A coupled electromechanical amalysis of piezoelectric layer bonded to an elastic substrate: Part I, development of governing equations. *International Journal of Solids & Structures*, vol. 40, pp. 6781–6797.